32ND INTERNATIONAL COSMIC RAY CONFERENCE, BEIJING 2011

Back-tracking studies of the arrival directions of UHECR detected by the Pierre Auger Observatory

MICHAEL S. SUTHERLAND[1], FOR THE PIERRE AUGER COLLABORATION[2]
[1]*Louisiana State University, Baton Rouge, LA 70803-4001, United States*
[2]*Observatorio Pierre Auger, Av. San Martín Norte 304, 5613 Malargüe, Argentina*
(Full author list: http://www.auger.org/archive/authors_2011_05.html)
auger_spokespersons@fnal.gov

Abstract: The Pierre Auger Observatory has performed precise measurements of ultra-high energy cosmic rays (UHECRs) which carry information on their source and propagation environments. We present an analysis that explores various features of the geometry and intensity of magnetic fields that influence the trajectories of ultra-high energy cosmic rays. Under the hypothesis of pure primary protons at the energy of interest (i.e., above 50 EeV), using different catalog-based assumptions on sources and a variety of simplistic Galactic magnetic field (GMF) models, we backtrack the arrival directions of UHECRs observed with the Pierre Auger Observatory. We quantify self-consistency by comparing to results for a simulated set of isotropic directions. The obtained results represent an illustrative example of the potential of UHECR data for obtaining information on their origin, their propagation, and on the properties of the GMF.

Keywords: Ultra-High Energy Cosmic Rays, Pierre Auger Observatory, Magnetic Fields, Sources

1 Introduction

The observation of cosmic rays at the highest energies (UHECRs) and the precise measurement of their kinematic properties with the Pierre Auger Observatory enables approaches towards the fundamental questions on the UHECR origin and propagation. As the physics of particle propagation is well established through laboratory studies, comparison of UHECR measurements with astrophysical models constitutes a promising method for obtaining information on their sources and characterization of the magnetic fields traversed from those sources.

In this contribution, we present a first comparison of the Pierre Auger dataset with specific astrophysical models using an analysis method previously shown in [1] which has been extended in [2]. For a variety of hypothesis sets each comprised of Galactic magnetic field (GMF) models and UHECR sources, we perform a search for hypothesis set self-consistency when folded with the Pierre Auger measurements. The primary focus of this analysis is the GMF, whose properties have been measured previously using Faraday rotation and starlight polarization techniques [3, 4, 5, 6, 7]. Observed UHECRs are backtracked as single-charged particles through simple GMF geometries. In order to quantify a self-consistent hypothesis set we compare the resulting particle trajectories with source candidates using different catalogues and test this source correlation against the expectation of backtracked isotropic simulations.

The paper is structured as follows. We first introduce the method for determining hypothesis set self-consistency. We then specify the data set recorded by the Pierre Auger Observatory. In the third section we explain the different astrophysical model components of catalog-based sources and GMF parameterizations. The fourth section contains results obtained by scanning the different models in comparison to the hypothesis of isotropic expectations. Finally, we discuss the effects of the measurement uncertainties and the influence of additional magnetic turbulent components on a representative hypothesis set.

2 Method Description

The Field Scan Method (FSM) [2] assesses the self-consistency of a set of UHECR and GMF hypotheses. It compares the correlation between source locations and event trajectories after backtracking both a dataset of interest (DOI) and isotropic simulations. The results of the method are explicitly dependent on the choice of the individual components. The comparison with isotropy accounts for chance correlation with sources as well as for lensing due to the GMF configuration, building on the procedure used in [1]. The test statistic (TS)

$$\Psi_i = \Theta_i/(1+\Delta_i) \quad (1)$$

is computed for each event i, where Δ_i is the deflection magnitude and Θ_i the angular distance to the nearest source

object. A Kolmogorov-Smirnov (KS) test is performed between the DOI and isotropic TS distributions, using the largest signed difference $D_{\max}$ between the cumulative TS distributions. $|D_{\max}|$ maps to the probability $P_{\rm KS}$ that the TS distributions are drawn from the same parent distribution.

The hypothesis set is deemed *self-consistent* to the extent that the $P_{\rm KS}$ value indicates *inconsistency* with isotropy and that the DOI correlates well with the source hypothesis. A large positive $D_{\max}$, resulting in small $P_{\rm KS}$, located at a small TS value indicates that the DOI better correlates with the source hypothesis than the isotropic expectation and is inconsistent with the isotropic expectation. Conversely, if the dataset differs little from the isotropic expectation (small $D_{\max}$ and large $P_{\rm KS}$), then one or more of the hypothesis components may be incorrect, or perhaps the method is probing a regime where self-consistency cannot be identified (e.g., strong lensing that hinders identification of significant source correlation beyond the isotropic expectation). Positive $D_{\max}$ at large TS values and any negative $D_{\max}$ are also indicators of these scenarios.

3 Dataset

The Pierre Auger Observatory is a hybrid air shower detector located in Malargüe, Argentina. The Surface Detector (SD) consists of a 3000 km^2 array of 1660 surface detectors overlooked by the 27 fluorescence telescopes of the Fluorescence Detector (FD) grouped at 4 sites on the array boundary. This allows for complementary measurements of the lateral distribution of air shower particles at ground level by the SD and the longitudinal development of the air shower by the FD.

The data used here consists of 126 events recorded between 1 January 2004 and 31 December 2010 with reconstructed energies greater than 50 EeV and zenith angles smaller than 60°. These events are required to have at least five active detectors surrounding the detector reporting the highest signal and that the reconstructed core location lie within an equilateral triangle of active detectors.

4 Hypothesis Sets

4.1 Composition

The data and simulations are hypothesized here to be entirely protons ($Z_p = 1$). This approach appears limited with respect to measurements of the air shower characteristics which are consistent with a heavy composition at the highest energies [8]. Another measurement, namely the correlation of the observed arrival direction at the highest energies ($E \geq 55$ EeV) with extragalactic objects, is suggestive of a light composition and deflection magnitudes of order a few degrees [9].

Parameter	Min. Value	Max. Value	Step Size
$B_\odot$	-2.0 μG	10.0 μG	0.5 μG
p	-20°	-1°	1°
Z_1	0.2 kpc	4.0 kpc	0.2 kpc

Table 1: GMF Parameter Space Grid

4.2 Source Distributions

Choices for source distributions are drawn from different expectations. Four (4) distinct source distributions are assumed. We use Active Galactic Nuclei (AGN) from the Veron Catalog of Quasars & AGN, 12th Edition [10] (VCV). The 39 month SWIFT-BAT catalog [11] provides a comprehensive all-sky AGN survey in hard X-rays (Swift39). We also use the 2MRS compilation [12] of redshifts of the $K_{mag} < 11.25$ brightest galaxies from the 2MASS catalog [13]. This catalog provides an excellent tracer of the nearby matter distribution in the universe. We apply a variety of redshift cuts $z \leq z_{cut}$ to these three catalogs using the values $z_{cut} = (0.010, 0.011, ..., 0.024)$. Additionally for the 2MRS catalog, we apply an absolute brightness cut that scales with the redshift cut to prevent a bias towards faint galaxies at small distances (2MRS-VS); this cut would be equivalent to $M_K < -25.25$ at redshift $z = 0.048$ (d =200 Mpc). Finally, the radio galaxy Centaurus A is treated as a sole source (CenA).

4.3 Galactic Magnetic Field Models

In this work, we implement logarithmic symmetric spiral field models as models for the large-scale regular GMF. Logarithmic symmetric spirals represent *a priori* reasonable models for the functional form of the regular component of the Galactic magnetic field [14]. Such spiral models have been explored in previous studies of UHECR deflection in GMF models [15, 16, 17, 18]. Turbulent and halo components are not considered here, nor are extra-galactic magnetic fields [19, 20, 21].

We investigate the axisymmetric (ASS_A) and bisymmetric models (BSS_S) as described in [16]. These are smoothed versions of models given by [15]. The ASS_A (BSS_S) model exhibits (anti-) symmetry under rotations of π around the Galactic pole and is antisymmetric (symmetric) under reflection across the Galactic mid-plane. Three model parameters are scanned using the volume defined by the range shown in Table 1: the field strength in the local solar vicinity $B_\odot$, the pitch angle p giving the orientation of the local field vector in the mid-plane, and the scale height Z_1 giving the exponential attenuation of the field strength with distance from the mid-plane. All other parameters are the same as in [16].

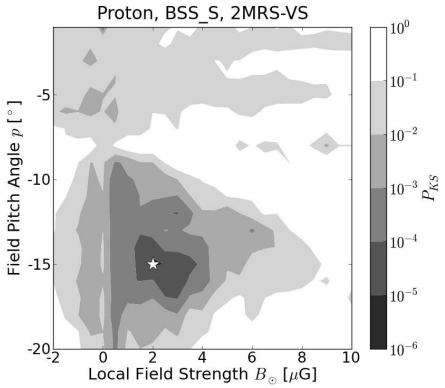

Figure 1: $P_{\rm KS}$ contours for (BSS_S, Proton, 2MRS-VS) hypothesis set with $z_{cut} = 0.017$ at $Z_1 = 2.0$ kpc.

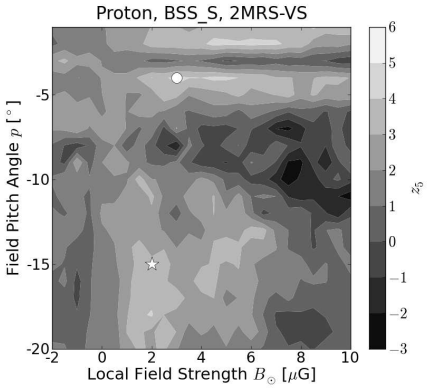

Figure 2: Deviation from isotropic source correlation expectation for (BSS_S, Proton, 2MRS-VS) hypothesis set with $z_{cut} = 0.017$ at $Z_1 = 2.0$ kpc.

5 Results

The isotropic TS expectation is comprised of 100 simulations[1] generated by randomly reassigning event directions while respecting the detector exposure. Data and simulations are backtracked using the *CRT* propagation code [22].

Regions of hypothesis set self-consistency will appear as sets of neighboring points in the GMF parameter space indicating comparable small values of $P_{\rm KS}$, positive $D_{\rm max}$ and excess source correlation at small angular scales. Such regions are observed for sets comprised of both field models and the VCV, Swift39, and 2MRS-VS catalogs implementing redshift cuts between roughly 0.014 and 0.020. For the BSS_S model, these regions typically encompass positive field strengths less than about +4 μG and $p \approx -15^\circ \pm$ few degrees. Regions in the ASS_A parameter space are found for slightly smaller field strengths of the opposite sign, possibly resulting from a nearby field reversal inside the solar Galactic orbit induced by the model change. Using smaller or larger redshift cuts, these regions are smaller in extent and shallower in $P_{\rm KS}$ as well as shifted within the parameter space. Values of the scale height range from 1 - 3 kpc depending on the specific hypothesis set. These parameter values are compatible with those determined from radio astronomical measurements [3, 4, 6].

Figure 1 depicts an example self-consistent region within the (Proton, BSS_S, 2MRS-VS) hypothesis set. The smallest value of $P_{\rm KS}$ in this set is 6.2×10^{-6} at (2.0 μG, -15.0°), marked by the white star. Low values of $P_{\rm KS}$ indicate that the dataset is behaving differently than isotropy for an extensive region of parameter space, although themselves do not indicate actual source correlation.

Figure 2 depicts the dimensionless deviation from the isotropic expectation of source correlation within 5°, defined as $z_5 = (n_5^d - n_5^i)/s_5^i$, for the same hypothesis set. At each point n_5^d is the number of dataset events. The number of isotropic events is calculated for each of the 100 simulations; n_5^i and s_5^i are the mean and standard deviation of this distribution. At (2.0 μG, -15.0°) marked by the white star, $z_5 = 3.25$, resulting from 36 events correlating within 5° compared to 21.47 expected. The combination of this small-scale correlation and small $P_{\rm KS}$ indicates that this hypothesis set is self-consistent. Points in the surrounding parameter space possess similar n_5^d and P_{KS} values. Larger z_5 are observed outside this region although marginal TS inconsistency with isotropy is found using $P_{\rm KS}$. One such point is (3.0 μG, -4.0°) marked by the white circle where 35 events comprise n_5^d (18.76 expected) giving $z_5 = 4.35$ but $P_{\rm KS} = 0.051$. Here the sky distribution of the data closely matches that of the isotropic simulations.

Hypothesis set combinations with Cen-A indicate no regions of self-consistency for either field model. The method returns a minimum $P_{\rm KS}$ value of 0.3% (0.05%) for the BSS_S (ASS_A) model. No parameter point in either hypothesis set returns $n_5^d \geq 12$ and large z_5 is not observed in conjunction with small $P_{\rm KS}$.

We note that the average $P_{\rm KS}$ for $B_\odot = 0$ μG in Figure 1 is 0.0123 indicating marginal inconsistency with isotropy. This is in accordance with a previous study of correlations of UHECR arrival directions with extragalactic objects reported in [9] using similar catalogs.

5.1 Energy and Angular Resolutions

We also investigate the effects of the energy and angular resolutions to determine the robustness of $P_{\rm KS}$. The Auger Observatory energy (σ_E) and angular (σ_ψ) resolutions are 15% and 0.9° [23, 24]. 10^3 "mock" datasets are generated where the event energies and directions are simultaneously resampled from gaussian distributions with widths σ_E and σ_ψ centered on the reconstructed energies and arrival directions, respectively. Then, 100 isotropic simulations are constructed for each "mock" dataset by keeping the resampled energies and reassigning an exposure-modulated isotropic direction for each event. A $P_{\rm KS}$ distri-

1. Simulations are unique for each parameter point. For $B_\odot = 0$ μG this will naturally induce variation in $P_{\rm KS}$.

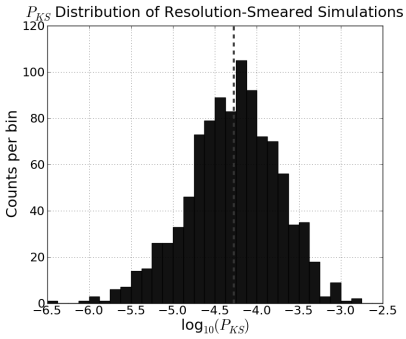

Figure 3: $P_{\rm KS}$ distribution of resolution-smeared "mock" datasets. The $P_{\rm KS}$ value for the unsmeared dataset is depicted by the vertical dotted line.

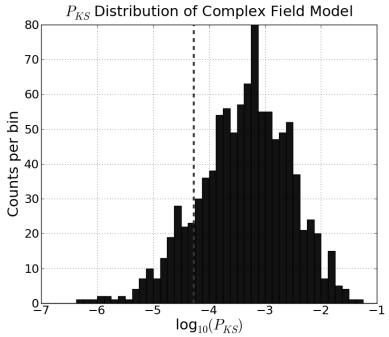

Figure 4: $P_{\rm KS}$ distribution for the regular plus turbulent GMF model. The $P_{\rm KS}$ value for the regular component-only model is depicted by the vertical dotted line.

bution sharply peaked about the value calculated using the reconstructed energy and direction would indicate strong robustness against experimental uncertainties. Figure 3 shows the $P_{\rm KS}$ distribution of the (Proton, BSS_S, 2MRS-VS) hypothesis set under $z_{cut} = 0.017$ for $(B_\odot,\ p,\ Z_1) = (2.0\ \mu{\rm G}, -15^\circ,\ 3.0\ {\rm kpc})$. The determination of self-consistency using the reconstructed energies and directions appears robust against the experimental resolutions.

5.2 Turbulent GMF Component

The addition of a turbulent field component is expected to induce isotropization with respect to the hypothesized source distribution. We compare the $P_{\rm KS}$ distribution of 10^3 realizations of a GMF with regular and turbulent components to the $P_{\rm KS}$ value of the sole regular field. The regular component is the same as in Section 5.1. The turbulent component consists of independent spherical cells of varying sizes drawn from a gaussian distribution with mean 0.1 kpc and rms 0.06 kpc. The field within individual cells has constant magnitude and direction, which is drawn from a gaussian distribution centered at $2.5\ \mu$G with rms $1\ \mu$G. Figure 4 shows the $P_{\rm KS}$ distribution for a particular BSS_S and 2MRS-VS hypothesis set. The addition of a turbulent component tends to strongly isotropize the data.

6 Conclusion

In this contribution we have presented a comparison of the Pierre Auger data with specific astrophysical models of the origin, composition, and propagation of UHECRs putting special emphasis on the GMF. In the comparisons we folded the measurements with the astrophysical hypothesis sets and performed a quantitative search for self-consistency. Interesting self-consistent descriptions are found for GMF parameter values that are consistent with contemporary radio astronomical measurements. By scanning a broad phase space of conventional GMF model parameters and several cosmic ray source hypotheses, we have shown an illustrative example of the potential of UHECR precision measurements to obtain new and important information on the fundamental characteristics of the high energy universe.

References

[1] B. M. Baughman, for the Pierre Auger Collaboration, Proc. 31st ICRC, Łódź, Poland, 2009. arXiv:0906.2347 [astro-ph].
[2] B. M. Baughman *et al.*, submitted to Astropart. Phys., 2010.
[3] H. Men *et al.*, Astron. and Astrophys., 2008, **486**:819.
[4] X. H. Sun *et al.*, Astron. and Astrophys., 2008, **477**:573.
[5] S. A. Mao *et al.*, Astrophys. Journ., 2010, **714**:1170.
[6] C. L. Van Eck *et al.*, Astrophys. Journ., 2011, **729**:97.
[7] M. Haverkorn *et al.*, Space Sci. Rev., 2011, **3**:29.
[8] The Pierre Auger Collaboration, Phys. Rev. Lett., 2010, **104**:091101.
[9] The Pierre Auger Collaboration, Astropart. Phys., 2010, **34**:314.
[10] M. P. Veron-Cetty *et al.*. Astron. and Astrophys., 2006, **455**:773.
[11] G. Cusumano *et al.*, Astron. and Astrophys., 2010, **510**:A48.
[12] J. Huchra *et al.*, IAU Symp., 2005, **216**:170.
[13] T. H. Jarrett *et al.*, Astronom. J., 2000, **119**:2498.
[14] F. S. Tabatabaei *et al.*, Astron. and Astrophys., 2008, **490**:1005.
[15] T. Stanev. Astrophys. Journ., 1997, **479**:290.
[16] D. Harari *et al.*, JHEP, 1999, **8**:22.
[17] M. Kachelrieß *et al.*, Astropart. Phys., 2007, **26**:378.
[18] H. Takami *et al.*, Astrophys. Journ., 2008, **681**:1279.
[19] S. Das *et al.*, Astrophys. Journ., 2008, **682**:29.
[20] D. Ryu *et al.*, Science, 2008, **320**:909.
[21] K. Dolag *et al.*, JCAP, 2009, **01**:33.
[22] M. S. Sutherland *et al.*, Astropart. Phys., 2010, **34**:198.
[23] The Pierre Auger Collaboration, Phys. Rev. Lett., 2008, **101**:061101.
[24] C. Bonifazi, for The Pierre Auger Collaboration, Nuc. Phys. B (Proc. Suppl.), 2009, **190**:20.